

## PATH INSTABILITY OF STRONGLY COLLAPSING BUBBLES DRIVING BY BI-FREQUENCY EXCITATION AT FINITE REYNOLDS NUMBERS

Ludmila M. Rechiman<sup>a,b</sup> and Fabián J. Bonetto<sup>a</sup>

<sup>a</sup>*Laboratorio de Cavitación y Biotecnología. Instituto Balseiro-UNCu-CNEA-CONICET. Centro Atómico Bariloche CP(R8402AGP), Río Negro, Argentina.*

<sup>b</sup>*Departamento Mecánica Computacional. Centro Atómico Bariloche CP(R8402AGP), Río Negro, Argentina.*

**Keywords:** Bubble dynamics, SBSL, Path instability, History force, Window method.

**Abstract.** In this work we present a study of the path instability that may be developed by strongly collapsing bubbles in highly viscous liquids. In particular we modify the driving pressure field by the addition of a high frequency component in order to suppress the pseudo-orbits. The condition of spatially fixed bubbles is necessary for an accurate experimental characterization of it. We investigate different modes for the high frequency component. In the present work we show that the spatial stabilization of the bubble could be obtained with different kind of harmonics. We also performed a sensibility analysis of the solutions under different phases between the low and high frequency components of the pressure field. Furthermore, we present a verification test to secure that the history force action cause the path instability and we also made a validation of the model with experimental measurements of the bubble radius driving with bi-harmonic and bi-frequency excitation showing a quite good agreement between them.

## 1 INTRODUCTION

The description of the behavior of dispersed bubbles immersed in different types of flows is an absolute interesting field in several technological areas, for instance in: cyclonic separators ([van Eijkeren and Hoeijmakers \(2010\)](#)), combustion of atomized fuel ([Chung \(1982\)](#)), tracers in turbulent flows ([Tchen \(1947\)](#)), ([Hinze \(1975\)](#)), ([Armenio and Fiorotto \(2001\)](#)), simulation of environmental flows ([Loth and Dorgan \(2009\)](#)), among others.

The dynamics of the translation of small dispersed spherical particles of fixed size in an unsteady flow and at low Reynolds numbers is well described by the Basset-Boussinesq-Oseen equation (BBOE) ([Maxey and Riley \(1983\)](#)). The BBOE equation considers the different hydrodynamic forces done by the fluid over the particles, and its resolution determine the trajectories of the particles. This approach allows to track in a Lagrangian manner the tracers or particles in unsteady flows. The hydrodynamic forces involved in the BBOE are: drag force, added mass force, buoyant force and Basset force.

Many expressions have been formulated for the Basset force for particles with fixed radius in a widely variety of flows ([Yang and Leal \(1991\)](#), [Mei et al. \(1994\)](#)). However, in the present work we are interesting on implement a model to describe the full motion of bubbles with variable radius due to its response to a pressure field imposed by ultrasound. In order to accomplish this, we have used a model for the history force developed by [Magnaudet and Legendre \(1998\)](#) which was elaborated for spherical bubbles with large volume variations.

The motivation of this problem is based on developing a numerical tool to study the possible “path instability” that may present bubbles driving by ultrasound in the context of Sonoluminescence study field ([Rechiman et al. \(2012b\)](#), [Rechiman et al. \(2013\)](#)).

The main issue within this field is the concentration of energy, and in order to rise this figure of merit, a key fact is to obtain more violent collapses by modifying the pressure field applied on the bubble. [Holzfuss et al. \(1998\)](#) proposed the bi-frequency excitation for it. With this type of excitation they obtained an increment of 300% in the intensity of light emitted by a sonoluminescent bubble of air immersed in water in comparison with the case of a single frequency excitation.

Subsequent works show by means of experimental fittings that the hydrodynamic theory is able to reproduce the experimental measurements of the temporal evolution of the radius of the bubble where bi-harmonic excitation was used, ([Hargreaves and Matula \(2000\)](#)).

[Moraga et al. \(2000\)](#) used a pressure field composed by the fundamental frequency and the 10<sup>th</sup> harmonic to obtained stable and sonoluminescent air bubbles in water. By the adjustment of the relative phase between the signals that composed the acoustic pressure field, they could increment the intensity of light emitted by the bubble, and they also determined that with the bi-frequency excitation a more efficient compression could be achieved respect to single frequency case and without modifying the maximum radius.

With the purpose that the bubbles will be more stable against shape perturbations and trying to minimize the amount of vapor of the liquid present at main collapse, new working fluids began to be used in the experiments. The main properties of the performed fluids are: low vapor pressure and more viscous than water. Liquids with these characteristics are for instance the concentrated sulfuric acid solutions ([Didenko et al. \(2000\)](#), [Flannigan and Suslick \(2005\)](#), [Hopkins et al. \(2005\)](#)). However, in the region of interest in the phase space of the problem, it was observed that bubbles did not were spatially stable and they described pseudo-orbits under a single driving frequency. This state was coined “moving-SBSL” (m-SBSL). The existence of this state makes the characterization of the bubbles more difficult, and in consequence this cause

the inability of determine in an indirect manner the reached temperature of the inside bubble contents. Besides, the bubbles move away from the central region of the resonator where the applied acoustic pressure is higher.

Later, the experimental suppression of the spatial trajectories of bubbles immersed in a concentrated sulfuric acid solution was first made by [Urteaga and Bonetto \(2008\)](#) by adding a second harmonic frequency to the acoustic field.

Recent investigations made by [Dellavale et al. \(2012\)](#), [Dellavale \(2012\)](#), revealed that the bi-harmonic excitation allows to trap and spatially stabilize bubbles in a highly viscous sulfuric acid solution for a small amount of dissolved gas in the liquid equivalent to 1 mbar ( $\frac{c_\infty}{c_0} \approx 0.001$ ). Under these conditions a boosting in the temperature of the inside bubbles contents was accomplished, and the predicted temperature was  $\sim 70000$  K. The remarkable fact of using highly degassed solutions is that higher acoustic pressures could be applied on the bubble and by means of the bi-frequency excitation the spatial trapping is possible.

In this context, the bi-harmonic excitation allows to enlarge the accessible cases able to experimentally characterize where the energy concentration rises in the phase space  $(p_a^b; R_0)$ . Because of this, in the present work we made a deeper study within the acoustic cavitation field, in order to study the presence of the path instability on bi-frequency driving bubbles, and show the developed tool to investigate the mechanisms that allows to spatially stabilize bubbles.

The work is organized in the following manner: in [Sec.\(2\)](#) we describe the numerical model that couples the radial dynamics and the translational motion of a single bubble immersed in an acoustic pressure field imposed by ultrasound. In [Sec.\(3\)](#) we show a verification procedure and a validation of the developed tool with experimental data. In [Sec.\(4\)](#) we show the numerical results regarding the path stability of a single bubble driving by bi-harmonic excitation. Finally in [Sec.\(5\)](#) we summarize our conclusions.

## 2 THE MODEL

In the present work we used the model presented in [Rechiman et al. \(2012b\)](#), [Rechiman et al. \(2013\)](#), to calculate the coupled radial and translational dynamics of a bubble. We deal with the particular case of a bubble driving by an intense acoustic pressure field so that the radial oscillations of the bubble are non-linear. The non-autonomous dynamical system that model the problem can be sum up in the following manner:

$$\left\{ \begin{array}{l} (1 - \frac{\dot{R}(t)}{c_l})R(t)\ddot{R}(t) + \frac{3}{2}\dot{R}^2(t)(1 - \frac{\dot{R}(t)}{3c_l}) = \frac{1}{\rho_l}(1 + \frac{\dot{R}(t)}{c_l})(p_g(R(t)) - p(r, t)) + \frac{R(t)p_g(R(t))}{\rho_l c_l} - \frac{4\nu_l \dot{R}(t)}{R(t)} - \frac{2\sigma}{\rho_l R(t)} \\ \dot{T}_b = -[\gamma(R, \dot{R}, T_b) - 1] \frac{3R^2(t)\dot{R}(t)}{R^3(t)-h^3} T_b(t) - \chi_g \frac{T_b(t)-T_0}{R^2(t)} \\ \vec{F}_b = -\frac{4}{3}\pi R^3(t)\nabla p(r, t) - \frac{2}{3}\pi\rho_l \frac{d(R^3(t)\vec{U}(r, t))}{dt} - 6\pi\rho_l\nu_l R(t)\vec{U}(r, t) - \frac{4}{3}\pi\rho_l R^3(t)\vec{g} - \\ -\theta_t(t)\theta_r(t)8\pi\rho_l\nu_l \int_0^t \frac{\alpha}{(a-1)\sqrt{\pi 9\nu_l} \int_\tau^t \frac{1}{R^2(s)} ds + \sqrt{\pi 9\nu_l} \int_\tau^t \frac{1}{R^2(s)} ds + a^2} \frac{d}{d\tau}(R(\tau)\vec{U}(r, \tau)) d\tau \end{array} \right. \quad (1)$$

The first equation of [Eqs.\(1\)](#) is the Rayleigh-Plesset-Keller equation [Keller \(1980\)](#) which describes the radial oscillations of the bubble. The second equation of [Eqs.\(1\)](#) is the energy equation assuming a Van der Waals gas inside the bubble and uniform profiles of pressure and temperature within the bubble. Finally, the third equation of [Eqs.\(1\)](#) is the translational equation

of the bubble which takes into account the following forces acting on it: primary Bjerknes force ( $\vec{F}_{Bjerknes}$  Leighton (1994)), added mass force ( $\vec{F}_{am}$  Landau and Lifshitz (1987)), steady-drag force ( $\vec{F}_{Drag}$  Batchelor (1967)), buoyant force ( $\vec{F}_{boy}$  Landau and Lifshitz (1987)) and history force ( $\vec{F}_{History}$  Magnaudet and Legendre (1998)). Further treatment of the history force kernel approximation can be found in Rechiman et al. (2012b), Rechiman (2013).

In the system represented by Eqs.(1),  $t$  is the time,  $R(t)$  is the radius of the bubble,  $\dot{R}(t)$  is the radial velocity of the bubble interface,  $\ddot{R}(t)$  is the radial acceleration of the bubble interface,  $\rho_l$  is the liquid density,  $c_l$  is the speed of sound in the liquid,  $\sigma$  is the surface tension,  $\nu_l$  is the kinematic viscosity of the liquid.  $T_b$  is the temperature of the gas contents inside the bubble,  $\gamma(R, \dot{R}, T_b)$  is the variable polytropic coefficient,  $\chi_g(t)$  denotes the thermal diffusivity of the gas,  $T_0$  is the ambient temperature and  $h$  is the Van der Waals hard core radius of the gas.  $r$  is the radial coordinate,  $r_b(t) = \sqrt{x(t)^2 + y(t)^2 + z(t)^2}$  is the distance from the center of the bubble to the origin of coordinates, which is located in the middle of a spherical resonator,  $x(t)$ ,  $y(t)$  and  $z(t)$  indicate the location of the center of the bubble in Cartesian coordinates,  $\vec{U}(r, t) = \vec{V}_b - \vec{u}_l(r, t)$  is the relative velocity between the bubble translational velocity and the liquid velocity and  $\vec{g}$  is the gravity acceleration.  $\theta_r(t)$  and  $\theta_t(t)$  are the switches for the activation or deactivation of the history force defined by Toegel et al. (2006).  $p_g(R(t))$  is the pressure of the gas contents inside the bubble and  $p(r, t)$  denotes the driving pressure field. The driving pressure field in the present work is composed by two parts: a low frequency component, which oscillates with the first eigenfrequency associated to a spherical resonator, and a high frequency component, which can oscillates with a harmonic frequency of the fundamental or with a non-harmonic frequency:

$$p(r, t) = p_\infty - \frac{\sin(k_0 r)}{k_0 r} p_a^0 \sin(2\pi f_0 t) - \frac{\sin(k_n r)}{k_n r} p_a^n \sin(2\pi n f_0 t + \phi) \quad (2)$$

In Eq.(2),  $p_\infty$  is the uniform static pressure, while the subindex “0” denotes the fundamental model and “ $n$ ” indicates the harmonic <sup>1</sup>.  $k_0 = \frac{2\pi f_0}{c_l}$  and  $k_n = \frac{2\pi n f_0}{c_l}$  are the wave numbers,  $r$  is the radial distance between the center of the bubble and the center of the resonator,  $f_0$  and  $f_n$  are the driving frequencies,  $\phi$  is the relative phase between the signals (is positive if the harmonic signal is forward the fundamental signal).  $p_a^0$  and  $p_a^n$  are the amplitudes of each component of the pressure field in the resonator center, and these two parameters can be controlled in the experiments. Is important to point out the difference between, the amplitudes of each component of the pressure field at the resonator center ( $p_a^0$  and  $p_a^n$ ), from the amplitudes of the pressure applied on the bubble at position  $r_b$  associated to each component, which we will indicate them in the following manner:  $p_a^{bLF} = \frac{\sin(k_0 r_b)}{k_0 r_b} p_a^0$  and  $p_a^{bHF} = \frac{\sin(k_n r_b)}{k_n r_b} p_a^n$ . If the bubble is not far away from the resonator center <sup>2</sup>, ( $p_a^{bLF}$  and  $p_a^{bHF}$ ) are similar to ( $p_a^0$  and  $p_a^n$ ) respectively. With the present model for the driving pressure field, it should be noticed that the spatial dependence of the fundamental and harmonic components are strictly radial.

The system of equations Eqs.(1) was solved by using the Runge-Kutta 4.5 adaptive step size algorithm, in which each integration step was determined by the doubling-stepping method Press et al. (1992). In this way we completely solved the three time scales involved in the problem which are:

<sup>1</sup> Harmonic frequency: is a frequency equivalent to an integer number ( $n$ ) of the fundamental frequency ( $f_0$ ). The last means:  $f_n = n f_0$ . In the case of no-harmonic frequencies, the argument of the function  $\sin()$  of the second term is  $f_{No\ Harm} \times t$ .

<sup>2</sup> a distance shorter than 2 mm for the range of parameters explored in the present work.

- Time scale associated with the main collapse of the bubble ( $\sim nseg.$ )
- Time scale associated with the expansion of the bubble during the rarefaction phase of the ultrasound ( $\sim \mu seg.$ )
- Time scale associated with the spatial trajectories of the bubble ( $\sim seg.$ )

The third equation of the system Eqs.(1) that governs the translational motion is an integrodifferential equation. One possible method to solve it is to evaluate the integral term of the history force model in each time step of the integration of the whole coupled system of equations given by Eqs.(1). To evaluate the integral in each time step, 15 variables involved in the history force integrand were stored:  $t$ ,  $R(t)$ ,  $\dot{R}(t)$ ,  $u_l^x(r, t)$ ,  $u_l^y(r, t)$ ,  $u_l^z(r, t)$ ,  $\dot{u}_l^x(r, t)$ ,  $\dot{u}_l^y(r, t)$ ,  $\dot{u}_l^z(r, t)$ ,  $\dot{x}_b(t)$ ,  $\dot{y}_b(t)$ ,  $\dot{z}_b(t)$ ,  $\ddot{x}_b(t)$ ,  $\ddot{y}_b(t)$  y  $\ddot{z}_b(t)$ <sup>3</sup>.

The strict manner to make the integration of the history force, will be to store the whole evolution of the bubble from the very beginning of the simulation. However, this way of calculation have several draw backs: the large amount of time required to make the calculations in each time step of integration of the complete system, the large amount of storage memory and the model of the history force used in the present work is valid a finite time backwards as it was indicated by [Magnaudet and Legendre \(1998\)](#).

In this sense, with the purpose of store a lower amount of data and make the integration over a shorter period of time, one possible method is to apply the “*window method*” in which a finite truncated time interval is considered.

This method was developed in first place by [Dorgan and Loth \(2007\)](#) to solve the integral of the Basset force over particles of fixed size, denser than the host liquid and in a range in which the fluid dynamic around the body could be described by a creeping flow motion. That work was also extended by [Loth and Dorgan \(2009\)](#) for the study of bubbles, and optimize in precision and time by [van Hinsberg et al. \(2011\)](#), but all those works are orientated to the study of translating bubbles with fixed size.

In the present work we implement the “*window method*” to solve the integral associated to the history force model. The history force integral, which it is solved in each step of the integration of the complete system, was made by using the two-points Newton-Cotes closed formula [Press et al. \(1992\)](#). This method was selected based on time computing restrictions, due to the history force integral is mainly composed by two integrals one inside the other, one depending on  $R(s)$  which is inside the integral over  $\tau$ . Both integration ranges,  $s$  y  $\tau$ , are the same and correspond to the selected window size (indicated by  $N$  points).

Figure (1) shows the scheme of calculation of the system of equations given by Eqs.(1).

### 3 VERIFICATION AND VALIDATION OF THE NUMERICAL CODE

#### 3.1 PATH INSTABILITY DUE TO THE ACTION OF THE HISTORY FORCE ON THE BUBBLE

[Toegel et al. \(2006\)](#) shows that the history force is the reason of the existence of the path instability of bubbles immersed in highly viscous fluids. In order to make a check of consistency, we simulate the same case with and without the history force term in the model. We have considered an argon bubble in SA85 solution with an ambient radius of  $R_0 = 9.0\mu m$ , which is driving by an acoustic pressure field which amplitude at the resonator center is  $p_a^0 \simeq p_a^b = 1.65$  bar and oscillates at  $f_0 = 30.0$  kHz. Based on the experiments, this case is associated with a

<sup>3</sup>Here the subindex “*l*” indicates “liquid”, while “*b*” indicates “bubble”.

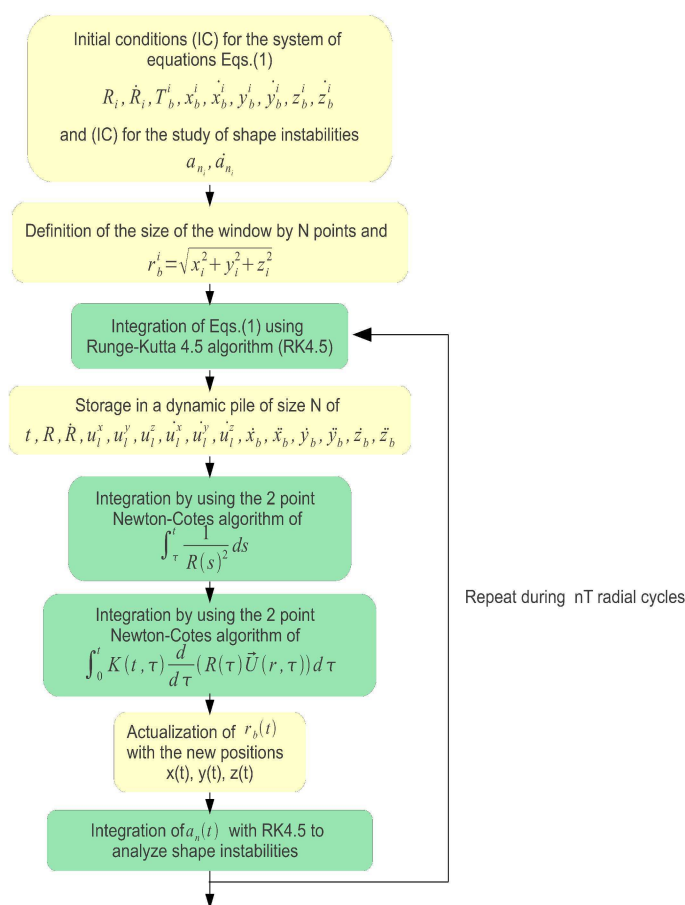


Figure 1: Calculation scheme of the system of equations given by Eqs.(1).

bubble which is path unstable. The initial conditions for both states are:  $R_i = R_0$ ,  $\dot{R}_i = 0.0 \frac{m}{s}$ ,  $T_b^i = 293.15$  K,  $x_i = 0.1$  mm,  $\dot{x}_i = 0.0 \frac{m}{s}$ ,  $y_i = -0.15$  mm,  $\dot{y}_i = 0.0 \frac{m}{s}$ ,  $z_i = 0.0$  mm,  $\dot{z}_i = 0.0 \frac{m}{s}$ . In the case displayed in Figure (2A) in which we have not included the history force in the model, it can be seen that the bubble moves to a levitation location above the origin of coordinates but without describing pseudo-orbits. On the other hand, in Figure (2B) we show that the inclusion of the history force term to the model cause the appearance of the path instability. In all the simulated cases the trajectories are contained in a bidimensional subspace.

### 3.2 VALIDATION OF THE NUMERICAL CODE WITH EXPERIMENTAL DATA

We have shown that the hydrodynamic force responsible for the path instability of bubbles driven by a pressure field imposed by ultrasound oscillating in the non-linear regime immersed in a highly viscous liquid, is the history force, (Toegel et al. (2006), Rechiman et al. (2013), Rechiman (2013)). Typically, the experimental characterization of the radial dynamic of a bubble requires that the bubble will be fixed in a spatial position. If this condition is accomplished, the temporal evolution of the bubble radius can be measured, and by fittings with a suitable numerical model, it can be determined the amplitude of the pressure applied on bubble wall, the amount of non-condensable gas inside it and the temperature reached by the bubble contents.

Three different methods have been applied in order to get spatially stationary bubbles: I) keeping the amplitude of the pressure field below a certain threshold, II) using strongly degassed liquid and III) using multi-frequency excitation, harmonic in most of the cases. In particular, in the

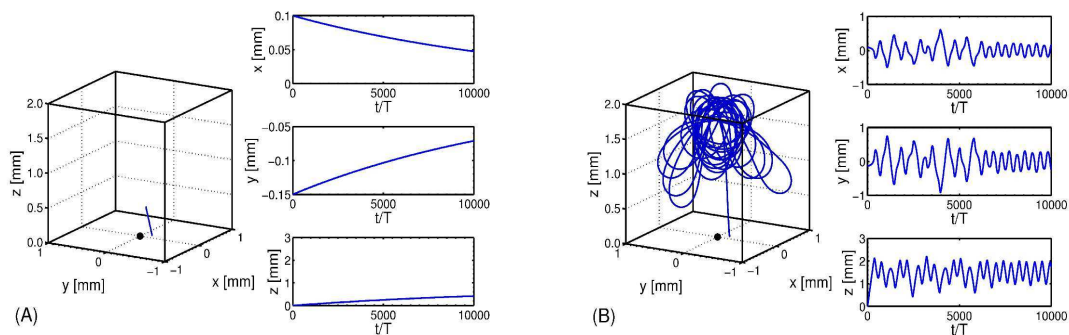


Figure 2: Influence of the history force acting on an argon bubble in SA85 which ambient radius is  $R_0 = 9.0\mu\text{m}$ . The bubble is driving by an acoustic pressure field which amplitude at the resonator center is  $p_a^0 \simeq p_a^b = 1.65$  bar and oscillates at a frequency equal to  $f_0 = 30.0$  kHz. (A) Without including the history force term in the translational equation. (B) Including the history force in the model.

present work the suppression of the pseudo-orbits will be made by bi-frequency excitation, and by strongly degassed liquid in combination with the bi-frequency excitation.

In Figure (3A) we show an experiment made by Dellavale (2012), in which an argon bubble immersed in a SA85 solution driving by a pressure field which oscillates at 30 kHz in a spherical resonator, is in the m-SBSL state (moving Single Bubble SonoLuminescence). Figure (3B) shows that the addition of 7<sup>th</sup> harmonic to the driving pressure field cause the suppression of the pseudo-orbits <sup>4</sup>.

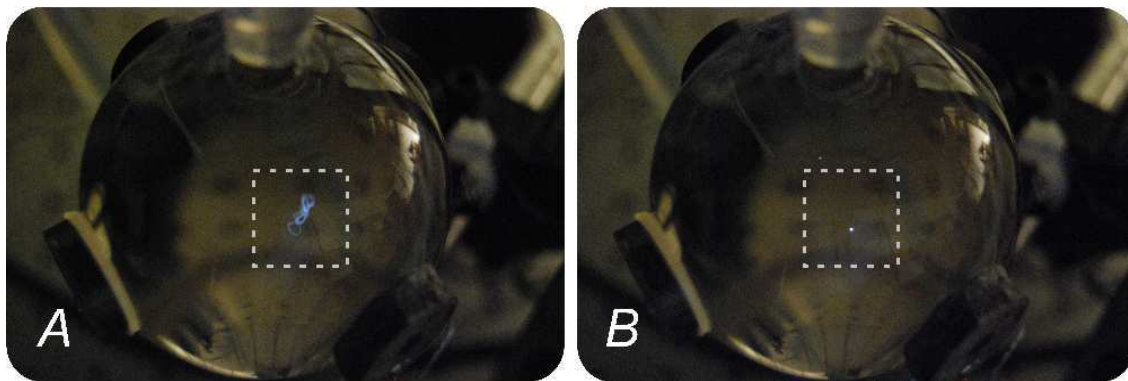


Figure 3: (A) Argon bubble moving in SA85 driving with the frequency associated with the first normal mode of a spherical resonator ( $f_0 = 29.2$ ) kHz. (B) Spatially fixed bubble due to the addition of a second component to the pressure field with a harmonic frequency ( $7f_0$ ). Both pictures were taken with a Nikon D50 camera, with a totally open diaphragm and with an integration time of 1 second Dellavale (2012). The concentration of dissolved gas in the liquid was equivalent to 16 mbar.

With the conditions of Figure (3B), the Figure (4) shows the measurements of the temporal evolution of the radius. The measurements were made by using the “Mie scattering” technique Urteaga (2008), Dellavale (2012), which allows to obtain a relative measurement <sup>5</sup> of the radius of the bubble as function of time. To illuminate the bubble an He-Ne Melles Griot laser (nominal

<sup>4</sup>We refer to “path suppression of the bubble” in the sense that a little movement of the bubble can exist, but the spatial scale is negligible or imperceptible for the measurements of the temporal evolution of the bubble radius.

<sup>5</sup>The intensity of light ( $I$ ) scattered by the bubble and collected by the photomultiplier tube follows this law:  $I(t) \propto R_{\text{bubble}}(t)^2$

power 30 mW) was used, and the scattered light was collected in a special angle by using a photomultiplier tube Oriel 77340, which has a characteristic response time of  $FWHM = 2.1 \text{ ns}$ . The fundamental driving frequency was similar to the one associated with the first normal mode of the resonator ( $f_0 = 29081 \text{ Hz}$ ), while the second frequency, was a harmonic frequency from the fundamental ( $f_7 = 7f_0 = 203567 \text{ Hz}$ ). It is important to point out that in this case the dissolved gas in the liquid was about 16 mbar. A concentration is considered “high” in SA85 solution if it is larger than 10 mbar (Dellavale (2012)), in which a bubble driven by only the fundamental frequency describes pseudo-orbits, and by the addition of a certain harmonic to the pressure field, the spatial fixing is possible (See Figure (3)B).

The selected parameters to characterize the bubble of Figure (4) and make the non-linear fitting are:  $R_0$ ,  $p_a^{bLF}$ ,  $p_a^{bHF}$  and  $\phi$ . We implement a code that allows to make multiple sweeps of the fitting parameters to minimize the  $\chi^2$  function. The figure of merit “ $\chi^2$ -function” is defined as:  $\chi^2 = \sum_{j=1}^N \left( \frac{R_j^{exp} - R_j^{model}}{\delta_j} \right)^2$ , where  $N$  is the amount of experimental points,  $R_j^{exp}$  indicates each experimental point of the measurement of the radius as function of time,  $\delta_j$  is the standard deviation associated to each experimental point and  $R_j^{model}$  is the radius of the bubble calculated by numerical integration.

Due to the fact that the translational dynamics does not cause major changes on the radial dynamics respect to the maximum radius, minimum radius and rebound structure, the fittings were made by suppressing the translational dynamics and the spatial dependence from the numerical model. This was made in order to reduce the computing times<sup>6</sup>.

Figure (4) shows that the fitting of the experimental data is quite good because it is able to reproduce the complex structure of the rebounds. This points out that the thermodynamical model used in this work for the evolution of the gas inside the bubble is a suitable model. Moreover, from the fitting it can be seen that the region in which the difference between the numerical and experimental results are larger is during main collapse. In particular, it can be seen that the experimental measurements obtained by using the “Mie scattering” technique does not reach the minimum radius predicted by the adjustment of the Rayleigh-Plesset-Keller equation. The same effect can be seen in experimental results obtained with the same technique reported by Lofstedt et al. (1995), Barber and Putterman (1992), Gompf and Pecha (2000). According to Brenner et al. (2002), the relation of proportionality between the intensity of collected light dispersed by the bubble and the square of the radius of the bubble is not longer valid during main collapse due to the refraction index of the inside bubble contents when is compressed, is unknown. Furthermore, the size of the bubble on those instants is of the same order of magnitude than the light’s wavelength. In spite of this, Urteaga and Bonetto (2008) made experiments in which they used another technique known as “fringe method” in order to measure the temporal evolution of the bubble radius. By using this method the radius of the bubble is measured in an absolute way and with higher accuracy, specially during main collapse. The results obtained by this procedure validate the hydrodynamic theory (RPKE) to describe the radius of the bubble. On the other hand, we also made fittings of an argon bubble in a SA85 solution but at a low gas concentration of dissolved gas in the liquid. At a pressure of 6 mbar of dissolved gas

<sup>6</sup>The grid used to make the fitting calculations to adjust 4 parameters ( $R_0$ ,  $p_a^{bLF}$ ,  $p_a^{bHF}$ ,  $\phi$ ), are  $10 \times 10 \times 10 \times 10$ , which represent 10000 simulations. In the case in which we consider the translational dynamics in the calculations, the steady state is reached after 5000 radial cycles, which are calculated in 10 hours. The last represent 100000 hours to make the calculations. By suppressing the translational dynamics to make the fittings, like it was made in previous works reported in the literature Puente (2005), Urteaga (2008), Dellavale (2012), the calculations to compute the fitting takes 5 hours approximately in a laptop with an INTEL core i5 processor. By applying this assumption, the model is reduced to consider a bubble immersed in an infinite liquid.

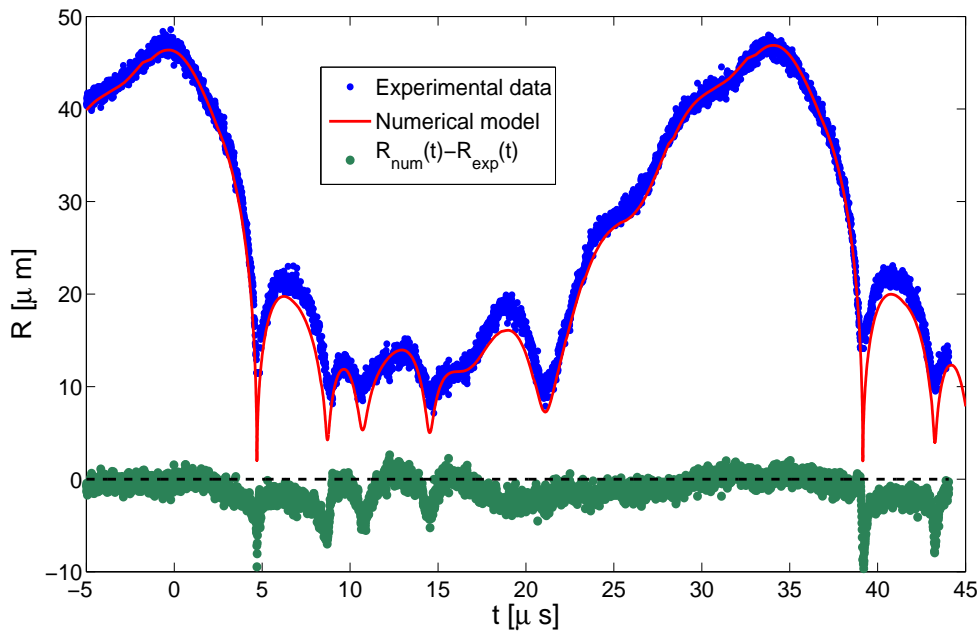


Figure 4: Temporal evolution of the radius of an argon SL bubble immersed in SA85. The concentration of dissolved gas in the liquid is approximately 30 mbar ( $\frac{c_\infty}{c_0} = 0.030$ ). The bubble is spatially stabilized by the bi-frequency excitation composed by the fundamental mode and the 7<sup>th</sup> harmonic:  $f_0 = 29081$  Hz,  $f_7 = 7f_0 = 203567$  Hz. (Blue dots) Experimental measurements made by using the “Mie scattering” technique. The measurements were obtained with a photomultiplier tube Oriel 77340 with a response time FWHM = 2.1ns. The dotted points are the result of the averaging of 10 measurements. (Red solid line) Non-linear fitting. The best parameters obtained by the  $\chi^2$  minimization procedure are:  $R_0 = (10.7 \pm 0.1)\mu\text{m}$ ,  $p_a^{bLF} = (1.34 \pm 0.02)$  bar,  $p_a^{bHF} = (1.19 \pm 0.02)$  bar,  $\phi = (1.80 \pm 0.01)$  rad. (Green dots) Indicates the difference between the radius predicted by the model and the corresponding experimental data.

in the liquid, which is a highly degassed case, the bubble can not be spatially trapped in the experiments (Dellavale (2012)). Because of this, an addition of a second component to the pressure field is needed in order to confine and stabilize the bubble under study.

Figure (5A) shows the experimental data associated with the temporal evolution of the radius of a bubble driving by bi-harmonic excitation composed by the fundamental mode at a frequency  $f_0 = 29075$  Hz and the 4<sup>th</sup> harmonic. It can be seen that the present model fits quite good the experimental data and capture the rebound phase in an accurate manner.

We have also made fittings of experimental data of an argon bubble in SA85 but driving by bi-frequency excitation (not harmonic). In this case the dissolved gas in the liquid was equivalent to 10 mbar, while the fundamental driving frequency is  $f_0 = 29116$  Hz and the not harmonic frequency is  $f_{NoHarm.} = 15$  kHz. In Figure (5B) it is shown the result of the fitting. It can be seen that the model is able to reproduce the *period-doubling* that is evident from the observation of experimental data for the mention kind of excitation.

## 4 NUMERICAL RESULTS FOR BI-FREQUENCY DRIVING BUBBLES

### 4.1 HARMONIC MODE EFFECT

In this section we show simulations made with the complete model for the experimental case displayed in Figure (4), and we analyze the effect of using different modes in order to get spatially stationary bubbles.

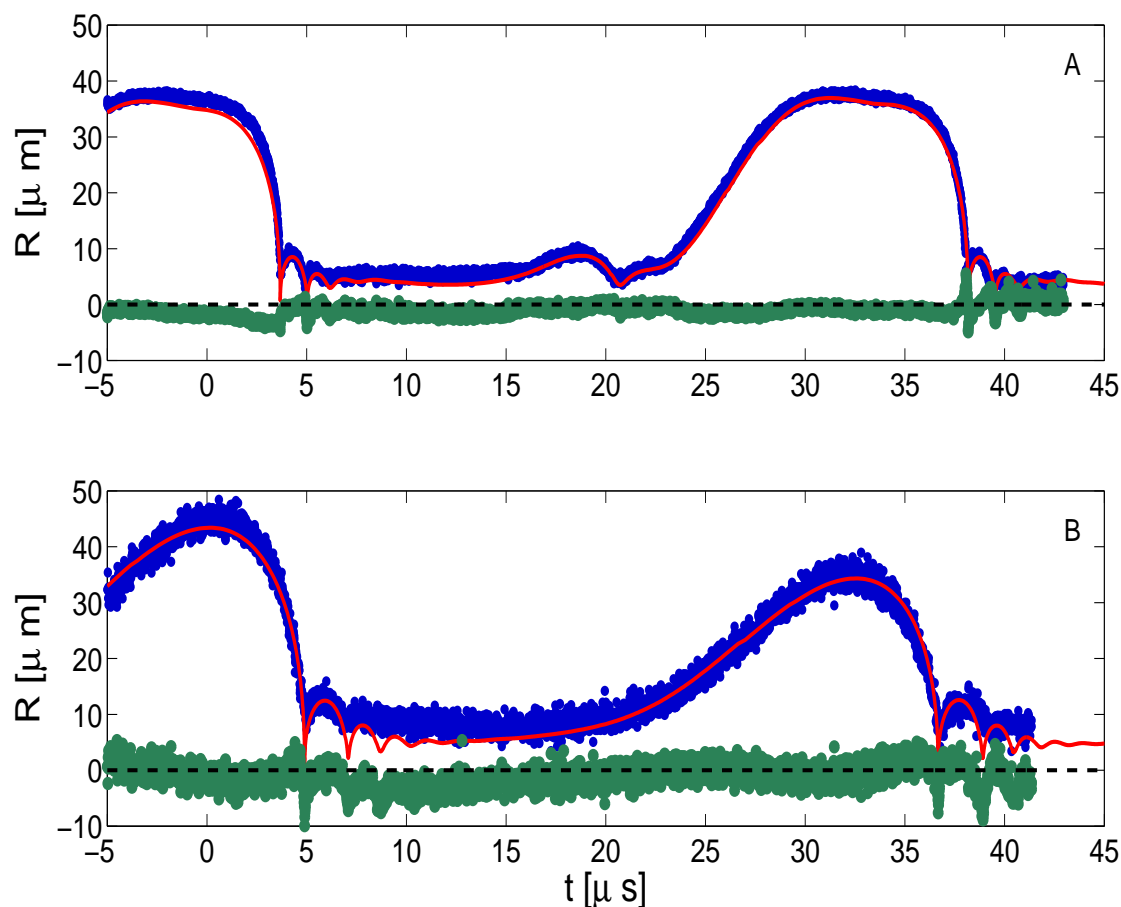


Figure 5: Temporal evolution of an argon bubble in SA85. (A) SL bubble under driving by a bi-harmonic excitation  $f_0 = 29075 \text{ Hz}$  and  $4f_0$ . The fitted parameters are:  $R_0 = (4.9 \pm 0.1)\mu\text{m}$ ,  $p_a^{bLF} = (1.50 \pm 0.02) \text{ bar}$ ,  $p_a^{bHF} = (0.92 \pm 0.02) \text{ bar}$ ,  $\phi = (-4.66 \pm 0.01) \text{ rad}$ . The concentration of gas dissolved in the liquid was equivalent to 6 mbar ( $\frac{c_\infty}{c_0} = 0.006$ ). (B) Bubble driving by bi-frequency excitation  $f_0 = 29116 \text{ Hz}$  y  $f_{NoArm.} = 15 \text{ kHz}$ . The fitted parameters are:  $R_0 = (6.3 \pm 0.1)\mu\text{m}$ ,  $p_a^{bLF} = (1.48 \pm 0.02) \text{ bar}$ ,  $p_a^{bHF} = (0.19 \pm 0.02) \text{ bar}$ ,  $\phi = (1.57 \pm 0.01) \text{ rad}$ . The concentration of gas dissolved in the liquid was equivalent to 10 mbar ( $\frac{c_\infty}{c_0} = 0.010$ ). The reference time  $t = 0$ , corresponds to the zero crossing with positive slope of the acoustic pressure in the fundamental mode. (Blue dots) Experimental data measured with the “Mie scattering” technique. (Red line) Non-linear fitting. (Green dots) Difference between the model and the experimental data.

In the sequence shown by Figure (6A-I) is displayed the path of an argon bubble in the experimental case of Figure (4). For the simulations we used the following input parameters, which are the results of the numerical fitting of experimental data:  $R_0 = (10.7 \pm 0.1)\mu\text{m}$ ,  $p_a^{bLF} = (1.34 \pm 0.02) \text{ bar}$ ,  $\phi = (1.80 \pm 0.01) \text{ rad}$ . At the beginning of the sequence, the bubble was only driving by the fundamental frequency, and gradually the amplitude of the high frequency component rises up to a value  $p_a^{bHF} = (1.19 \pm 0.02) \text{ bar}$ . It is relevant to point out from the observations of the simulations that the mean levitation position is quite near the origin of coordinates, and in consequence ( $p_a^0 \sim p_a^{bLF}$  and  $p_a^7 \sim p_a^{bHF}$ ). It can also be seen that the pseudo-orbits are suppressed when  $p_a^7$  rises, as well as the mean levitation approaches to the center (Rechiman et al. (2013)). This last effect could be explained based on the fact that the addition of a second component to the pressure field cause larger gradients. Larger spatial gradients of the pressure field implies that the averaged Bjerknes force in a radial period is more

intense in the case of a bi-harmonic driving bubble (spatially stable) respect to the case of a bubble driving by only the fundamental mode (moving bubble). On the other hand, the suppression of the pseudo-orbit is caused due to the maximum value of the added mass, which occurs at main collapse, diminishes. An important parameter to calculate in this kind of problem is the compression ratio, which for a bubble driving by only the fundamental mode is  $\frac{R_{max}}{R_{min}} = 20.6$ , while for the bubble driving by the fundamental mode and the 7<sup>th</sup> harmonic is  $\frac{R_{max}}{R_{min}} = 25.5$ .

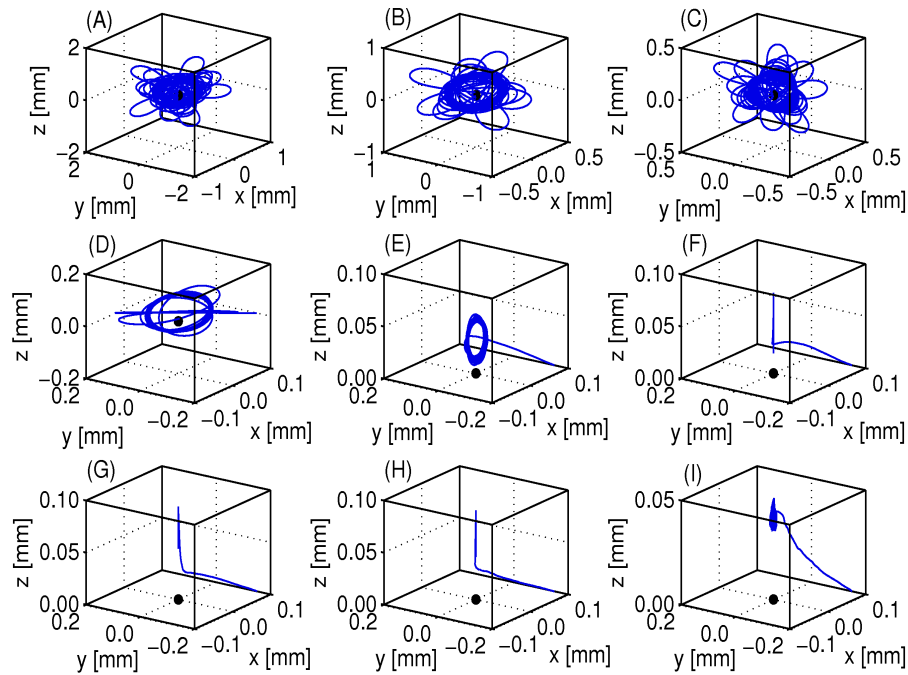


Figure 6: Simulated path of an argon bubble in SA85 solution with the same conditions of the experimental case shown in Figure (4). The characteristic parameters are:  $f_0 = 29081$  Hz,  $f_7 = 203567$  Hz,  $R_0 = 10.7\mu\text{m}$ ,  $p_a^{bLF} = 1.34$  bar. The sequence starts with a bubble driving by only the fundamental mode, and gradually the amplitude of the high frequency component of the pressure field rises. The initial conditions for the complete model are:  $R_i = R_0$ ,  $\dot{R}_i = 0.0\frac{\text{m}}{\text{s}}$ ,  $T_b^i = T_{liq}$ ,  $x_i = 0.10$  mm,  $\dot{x}_i = 0.0\frac{\text{m}}{\text{s}}$ ,  $y_i = -0.15$  mm,  $\dot{y}_i = 0.0\frac{\text{m}}{\text{s}}$ ,  $z_i = 0.0$  mm,  $\dot{z}_i = 0.0\frac{\text{m}}{\text{s}}$ . (A) Bubble driving by only the fundamental mode  $p_a^7 = 0.00$  bar. (B)  $p_a^7 = 0.15$  bar. (C)  $p_a^7 = 0.30$  bar. (D)  $p_a^7 = 0.45$  bar. (E)  $p_a^7 = 0.50$  bar. (F)  $p_a^7 = 0.55$  bar. (G)  $p_a^7 = 0.60$  bar. (H)  $p_a^7 = 1.05$  bar. (I)  $p_a^7 = 1.19$  bar.

In Figure (7) is displayed the sequence in which the amplitude of the second component of the pressure field given by the 4<sup>th</sup> mode rises. It can be seen that the model predicts that a nearly stationary bubble could be obtained but in a mean levitation position shifted from the pressure antinode (7I). In Figure (8) is shown the same sequence but using the 5<sup>th</sup> mode, which also allows to obtain spatially fixed bubbles but in a nearest position from the resonator center (8I). In Figure (9) is shown the sequence using the 6<sup>th</sup> mode, in which a similar behavior than in Figure (7I) is obtained. From this series of simulations it can be seen the high sensibility of the trajectories with the chosen mode for the high frequency component of the pressure field. The builded numerical tool allows to complement the kind of experiments done by Dellavale et al. (2012), Dellavale (2012), in which a sophisticated control system of the multi-frequency pressure field acting inside the resonator was developed.

It is worth to mention that in all presented cases, we have computed the shape instabilities along

the whole path to verify if the breakage of the bubble occurs. We have followed the scheme implemented by Rechiman et al. (2012a), but for periodically driving bubbles. The simulations presented in this work were found to be parametrically and Rayleigh-Taylor stable.

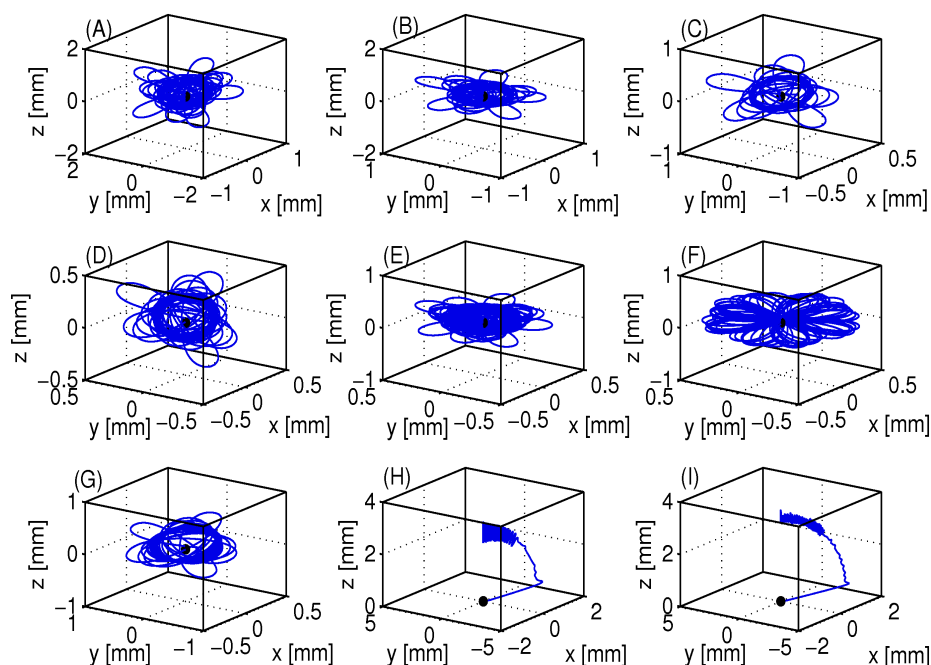


Figure 7: Simulated path of an argon bubble in SA85 solution with the same conditions of the experimental case shown in Figure (4), but using the 4<sup>th</sup> mode as a second component of the pressure field. The characteristic parameters are:  $f_0 = 29081$  Hz,  $f_4 = 116324$  Hz,  $R_0 = 10.7\mu\text{m}$ ,  $p_a^{bLF} = 1.34$  bar. The sequence starts with a bubble driving by only the fundamental mode, and gradually the amplitude of the high frequency component of the pressure field rises. The initial conditions for the complete model are:  $R_i = R_0$ ,  $\dot{R}_i = 0.0\frac{\text{m}}{\text{s}}$ ,  $T_b^i = T_{liq}$ ,  $x_i = 0.10$  mm,  $\dot{x}_i = 0.0\frac{\text{m}}{\text{s}}$ ,  $y_i = -0.15$  mm,  $\dot{y}_i = 0.0\frac{\text{m}}{\text{s}}$ ,  $z_i = 0.0$  mm,  $\dot{z}_i = 0.0\frac{\text{m}}{\text{s}}$ . (A) Bubble driving by only the fundamental mode  $p_a^4 = 0.00$  bar. (B)  $p_a^4 = 0.15$  bar. (C)  $p_a^4 = 0.30$  bar. (D)  $p_a^4 = 0.45$  bar. (E)  $p_a^4 = 0.50$  bar. (F)  $p_a^4 = 0.55$  bar. (G)  $p_a^4 = 0.60$  bar. (H)  $p_a^4 = 1.05$  bar. (I)  $p_a^4 = 1.19$  bar.

## 4.2 PHASE EFFECT

In the present section we show the sensibility of the solution with the phase between the signal associated with the high frequency component and the signal associated with the fundamental frequency component. We considered as a base case, the previous situation in which an  $R_0 = (10.7 \pm 0.1)\mu\text{m}$  argon bubble immersed in SA85 highly gassed solution ( $\sim 30$  mbar  $\frac{c_\infty}{c_0} = 0.030$ ) driving by  $f_0 = 29081$  Hz,  $p_a^{bLF} = (1.34 \pm 0.02)$  bar describe pseudo-orbits (Figure 6A) and by means of the addition of the 7<sup>th</sup> harmonic, the path is suppress (Figure 6I -Figure 10). In the last case the additional parameters are:  $f_7 = 7f_0 = 203567$  Hz,  $p_a^{bHF} = (1.19 \pm 0.02)$  bar,  $\phi = (1.80 \pm 0.01)$  rad.

In Figure (11) we show the solutions of the simulations made with the same input parameters than in Figure 10 but for different ( $\phi$ ) phases. It can be seen that the bubble no longer remains in a spatially fixed location like in the particular case of  $\phi = 1.80$  rad, and a widely variety of trajectories are obtained which indicates that the solution is highly sensible with the chosen phase.

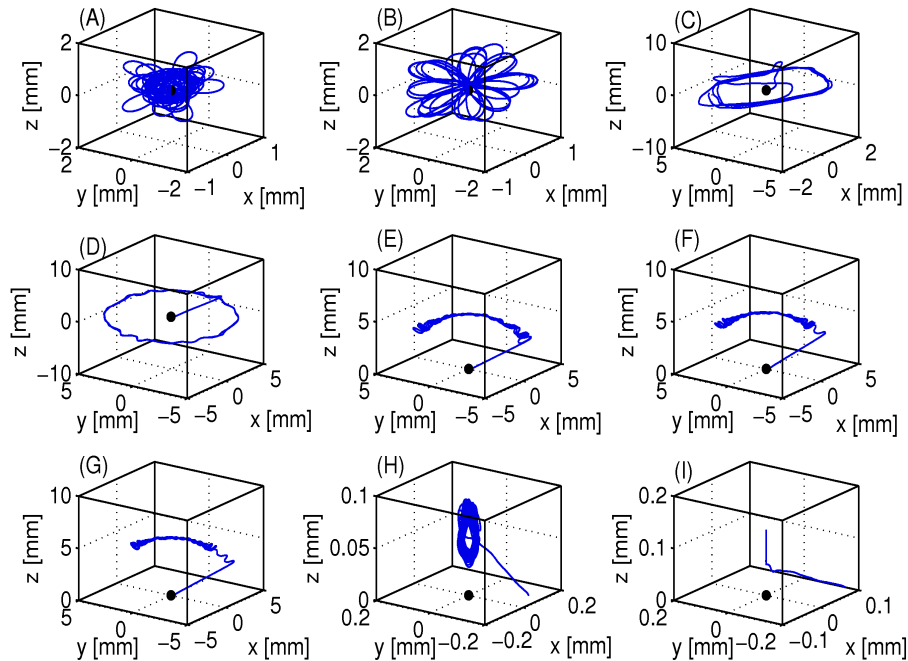


Figure 8: Simulated path of an argon bubble in SA85 solution with the same conditions of the experimental case shown in Figure (4), but using the 5<sup>th</sup> mode as a second component of the pressure field. The characteristic parameters are:  $f_0 = 29081$  Hz,  $f_5 = 145405$  Hz,  $R_0 = 10.7\mu\text{m}$ ,  $p_a^{bLF} = 1.34$  bar. The sequence starts with a bubble driving by only the fundamental mode, and gradually the amplitude of the high frequency component of the pressure field rises. The initial conditions for the complete model are:  $R_i = R_0$ ,  $\dot{R}_i = 0.0\frac{\text{m}}{\text{s}}$ ,  $T_b^i = T_{liq}$ ,  $x_i = 0.10$  mm,  $\dot{x}_i = 0.0\frac{\text{m}}{\text{s}}$ ,  $y_i = -0.15$  mm,  $\dot{y}_i = 0.0\frac{\text{m}}{\text{s}}$ ,  $z_i = 0.0$  mm,  $\dot{z}_i = 0.0\frac{\text{m}}{\text{s}}$ . (A) Bubble driving by only the fundamental mode  $p_a^5 = 0.00$  bar. (B)  $p_a^5 = 0.15$  bar. (C)  $p_a^5 = 0.30$  bar. (D)  $p_a^5 = 0.45$  bar. (E)  $p_a^5 = 0.50$  bar. (F)  $p_a^5 = 0.55$  bar. (G)  $p_a^5 = 0.60$  bar. (H)  $p_a^5 = 1.05$  bar. (I)  $p_a^5 = 1.19$  bar.

## 5 CONCLUSIONS

In the present work we have shown a validation of the numerical code with experimental data for spatially fixed bubbles. We have made non-linear fittings of an argon SL bubble driving by bi-harmonic and bi-frequency excitation. In particular, we have fitted experimental data of a stable argon bubble driving by the fundamental and the 7<sup>th</sup> harmonic. In this case, the liquid was highly gassed, then the spatial confinement and fixing could be attainable due to the addition of the second harmonic. It was shown that the numerical model correctly predicts the spatial fixing of the bubble in agreement with experimental observations. We have also made a fitting of a stable argon bubble driving by the fundamental and the 4<sup>th</sup> harmonic but in a highly degassed sulfuric acid solution. In this case the trapping of the bubble is not possible without a second harmonic in the pressure field. In order to explore further driving pressure fields, we have also fitted experimental data of an argon bubble driving by bi-frequency excitation (not-harmonic). In all cases, a quite good agreement between the numerical model and the experimental data was shown during most of duration of the radial period of the bubble except at main collapse due to the intrinsic nature of the experimental method used to measure the temporal evolution of the bubble radius.

We have shown the sensibility of the computed solutions with the chosen mode and the phase. The numerical simulations made allow us to determined that the addition of the 5<sup>th</sup> harmonic

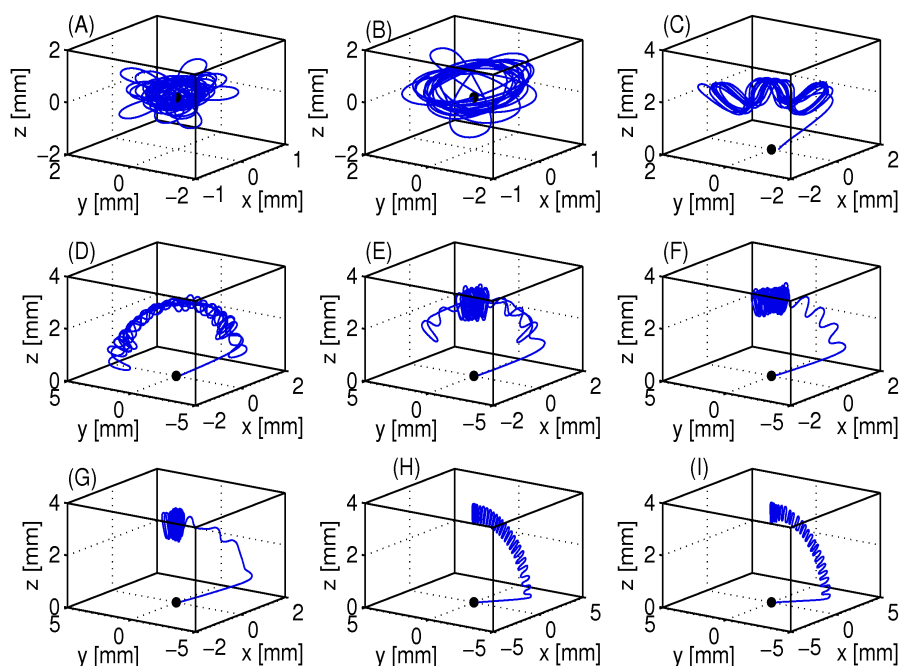


Figure 9: Simulated path of an argon bubble in SA85 solution with the same conditions of the experimental case shown in Figure (4), but using the 6<sup>th</sup> mode as a second component of the pressure field. The characteristic parameters are:  $f_0 = 29081$  Hz,  $f_6 = 174486$  Hz,  $R_0 = 10.7\mu\text{m}$ ,  $p_a^{bLF} = 1.34$  bar. The sequence starts with a bubble driving by only the fundamental mode, and gradually the amplitude of the high frequency component of the pressure field rises. The initial conditions for the complete model are:  $R_i = R_0$ ,  $\dot{R}_i = 0.0\frac{\text{m}}{\text{s}}$ ,  $T_b^i = T_{liq}$ ,  $x_i = 0.10$  mm,  $\dot{x}_i = 0.0\frac{\text{m}}{\text{s}}$ ,  $y_i = -0.15$  mm,  $\dot{y}_i = 0.0\frac{\text{m}}{\text{s}}$ ,  $z_i = 0.0$  mm,  $\dot{z}_i = 0.0\frac{\text{m}}{\text{s}}$ . (A) Bubble driving by only the fundamental mode  $p_a^6 = 0.00$  bar. (B)  $p_a^6 = 0.15$  bar. (C)  $p_a^6 = 0.30$  bar. (D)  $p_a^6 = 0.45$  bar. (E)  $p_a^6 = 0.50$  bar. (F)  $p_a^6 = 0.55$  bar. (G)  $p_a^6 = 0.60$  bar. (H)  $p_a^6 = 1.05$  bar. (I)  $p_a^6 = 1.19$  bar.

to the pressure field is able to trap and stabilize the bubble in the center of the resonator in agreement with previous experimental results reported by [Urteaga and Bonetto \(2008\)](#).

## ACKNOWLEDGMENTS

LMR acknowledges support from the Argentinian National Council for Scientific and Technological Research (CONICET). LMR thanks to Dr. Dellavale for providing the experimental data.

## REFERENCES

- Armenio V. and Fiorotto V. "The importance of the forces acting on particles in turbulent flows.". *Phys. Fluids*, 13:2437–2440, 2001.
- Barber B. and Putterman S. "Light Scattering Measurements of the Repetitive Supersonic Implosion of a Sonoluminescing Bubble.". *PRL*, 69, 1992.
- Batchelor G. "An introduction to fluid dynamics". Cambridge University Press, 1967.
- Brenner M.P., Hilgenfeldt S., and Lohse D. "Single-bubble sonoluminescence". *Rev. Mod. Phys.*, 74:425–484, 2002.
- Chung J.N. "The motion of particles inside a droplet.". *Transactions of the ASME*, 104:438–445, 1982.

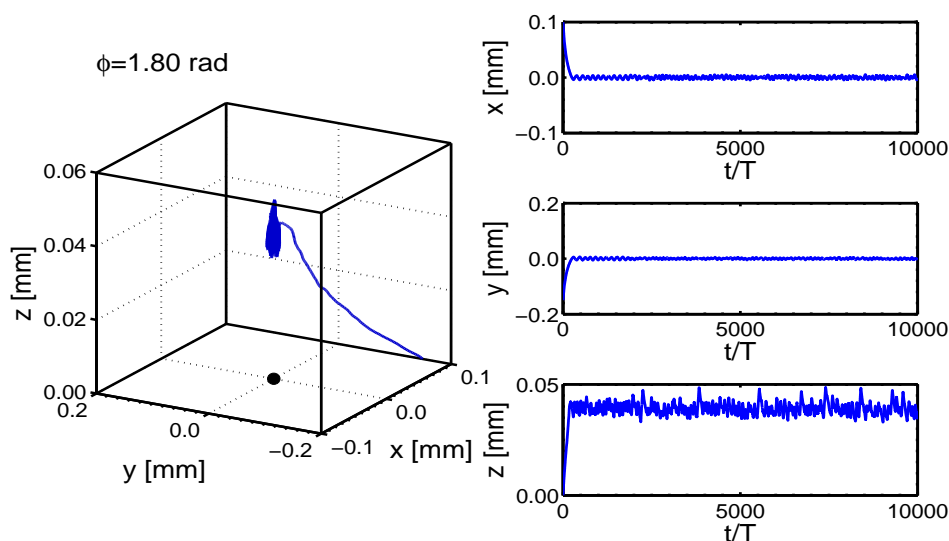


Figure 10: Suppressed pseudo-orbit of an argon bubble in SA85 driving by bi-harmonic excitation composed by the fundamental mode and the 7<sup>th</sup> harmonic. Is the case (I) of Figure (6). The phase between the harmonic signal and the fundamental mode is  $\phi = (1.80 \pm 0.01)$  rad.

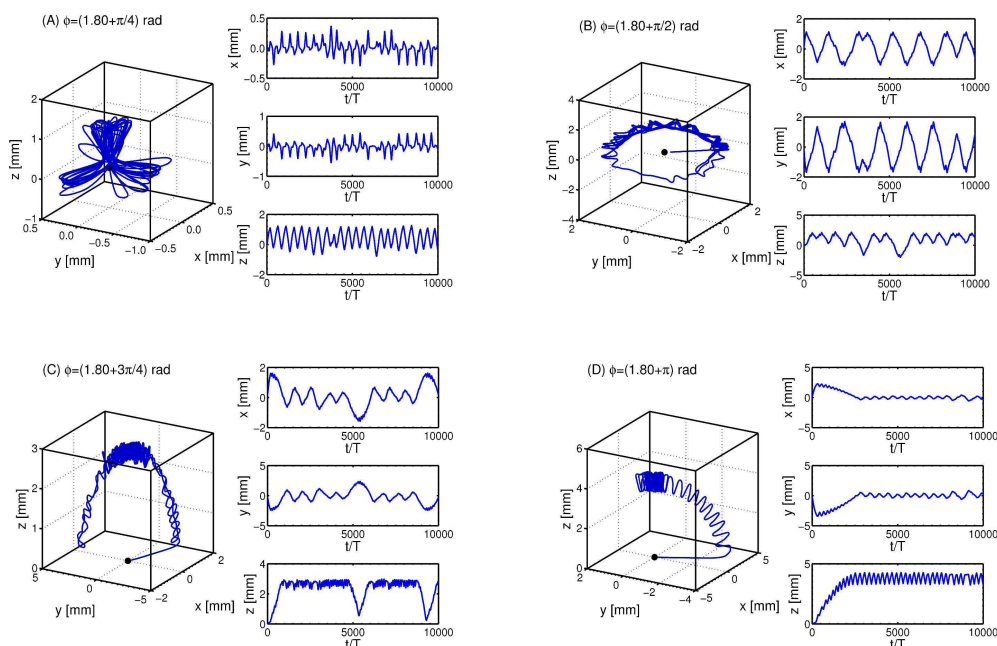


Figure 11: Trajectories of an argon bubble in SA85 driving by bi-harmonic excitation composed by the fundamental mode and the 7<sup>th</sup> harmonic. The pases between the harmonic signal and the fundamental mode are: (A)  $\phi = (1.80 + \frac{\pi}{4})$  rad. (B)  $\phi = (1.80 + \frac{\pi}{2})$  rad. (C)  $\phi = (1.80 + \frac{3\pi}{4})$  rad. (D)  $\phi = (1.80 + \pi)$  rad.

Dellavale D. "Concurrent signal processing algorithms with applications in sonoluminescence". Ph.D. thesis, Instituto Balseiro. Univ. Nac. Cuyo, 2012.

Dellavale D.H., Rechiman L.M., Rosselló J.M., and Bonetto F.J. "Upscaling energy concentration in multi-frequency single bubble sonoluminescence with strongly degassed sulfuric acid". *Phys. Rev. E*, 2012.

- Didenko Y., McNamara W.B., and Suslick K. "Molecular emission during single bubble sonoluminescence.". *Nature*, 407:877–879, 2000.
- Dorgan A. and Loth E. "Efficient calculation of the history force at finite Reynolds numbers.". *Int. J. Multiphase Flow*, 33:833–848, 2007.
- Flannigan D. and Suslick K. "Plasma formation and temperature measurement during single-bubble cavitation.". *Nature (London)*, 434:52–55, 2005.
- Gompf B. and Pecha R. "Mie scattering from a sonoluminescing bubble with high spatial and temporal resolution.". *Phys. Rev. E*, 61:5253–5256, 2000.
- Hargreaves K. and Matula T.J. "The radial motion of a sonoluminescence bubble driven with multiple harmonics.". *J. Acoust. Soc. Am.*, 107:1774–1776, 2000.
- Hinze J.O. "Turbulence". McGraw-Hill, 1975.
- Holzfluss J., Ruggeberg M., and Mettin R. "Boosting Sonoluminescence.". *PRL*, 81:1961–1964, 1998.
- Hopkins S., Putterman S., Kappus B., Suslick K., and Camara C. "Dynamics of a Sonoluminescing Bubble in Sulfuric Acid.". *PRL*, 95:254301, 2005.
- Keller J. "Bubble oscillations of large amplitude". *J. Acoustic Soc. Am.*, 68:628–633, 1980.
- Landau L.D. and Lifshitz E.M. "Fluid Mechanics". Pergamon Press., 1987.
- Leighton T. "The acoustic bubble". Academic Press, 1994.
- Lofstedt R., Weninger K., Putterman S., and Barber B.P. "Sonoluminescing bubbles and mass diffusion.". *Phys. Rev. E.*, 51:4400–4410, 1995.
- Loth E. and Dorgan A.J. "An equation of motion for particles of finite Reynolds number and size.". *Environ. Fluid Mech.*, 9:187–206, 2009.
- Magnaudet J. and Legendre D. "The viscous drag force on a spherical bubble with a time-dependent radius.". *Phys. Fluids*, 10:550–554, 1998.
- Maxey M. and Riley J. "Equation of motion for a small rigid sphere in a nonuniform flow.". *Phys. Fluids*, 26:883–889, 1983.
- Mei R., Klausner J.F., and Lawrence C.J. "A note on the history force on a spherical bubble at finite Reynolds number.". *Phys. Fluids*, 6:418–420, 1994.
- Moraga F.J., Taleyarkhan R.P., Lahey(Jr.) R.T., and Bonetto F.J. "Role of very-high-frequency excitation in single-bubble sonoluminescence.". *Phys. Rev. E.*, 62:2233–2237, 2000.
- Press W., Teukolsky S., and Vetterling W. "Numerical Recipes in C: The art of scientific computing". Cambridge University Press, 1992.
- Puente G.F. "Sonoluminiscencia y cavitación en burbujas: análisis dinámico y de estabilidad en regiones altamente no lineales". Tesis de doctorado, Instituto Balseiro. Univ. Nac. Cuyo, 2005.
- Rechiman L.M. "Numerical simulations of stability on acoustic and inertial cavitating bubbles.". Ph.D. thesis, Instituto Balseiro. Univ. Nac. Cuyo, 2013.
- Rechiman L.M., Bonetto F.J., and Rosselló J.M. "Effect of the Rayleigh-Taylor instability on maximum reachable temperatures in laser-induced bubbles.". *Phys. Rev. E.*, 86:027301, 2012a.
- Rechiman L.M., Dellavale D., and Bonetto F.J. "Path suppression of strongly collapsing bubbles at finite and low Reynolds numbers.". *Phys. Rev. E*, 2013.
- Rechiman L.M., Dellavale D.H., and Bonetto F.J. "Numerical description of moving single bubble sonoluminescence state in sulfuric acid". *Proceedings of the MECOM 2012. Volume XXXI. Asociación Argentina de Mecánica Computacional.*, pages 255–278, 2012b.
- Tchen C. "Mean Value and Correlation Problems connected with the Motion of Small Particles suspended in a turbulent fluid.". Phd thesis, Delft University, 1947.

- Toegel R., Luther S., and Lohse D. "*Viscosity destabilizes sonoluminescing bubbles.*". *PRL*, 96:114301/1–114301/4, 2006.
- Urteaga R. "Concentration of Energy in Sonoluminescence". Ph.D. thesis, Instituto Balseiro. Univ. Nac. Cuyo, 2008.
- Urteaga R. and Bonetto F. "*Trapping an Intensely Bright, Stable Sonoluminescing Bubble.*". *PRL*, 100:074302, 2008.
- van Eijkeren D.F. and Hoeijmakers H.W.M. "*Influence of the history term in a Lagrangian method for oil-water separation.*". *7th International Conference on Multiphase Flow. ICMF 2010*, 2010.
- van Hinsberg M., ten Thije Boonkkamp J., and Clercx H. "*An efficient, second order method for the approximation of the Basset history force.*". *J. Comp. Phys.*, 230:1465–1478, 2011.
- Yang S. and Leal L. "*A note on memory-integral contributions to the force on an accelerating spherical drop at low Reynolds number.*". *Phys. Fluids*, 3:1822–1824, 1991.